Title	Hole detrapping type persistent phosphors of RE2O2S (RE= La, Gd, Y, Lu) doped with Eu3+-Pr3+ and Eu3+-Tb3+
Author(s)	Hashimoto, Atsunori; Ueda, Jumpei; Aoki, Yasushi; Dorenbos, Pieter; Tanabe, Setsuhisa
Citation	The Journal of Physical Chemistry C, 127(31): 15611-15619
Issue Date	2023-07-26
Type	Journal Article
Text version	author
URL	http://hdl.handle.net/10119/19326
Rights	Atsunori Hashimoto, Jumpei Ueda, Yasushi Aoki, Pieter Dorenbos, Setsuhisa Tanabe, The Journal of Physical Chemistry C, 2023, 127, 31, 15611–15619. This document is the Accepted Manuscript version of a Published Work that appeared in final form in The Journal of Physical Chemistry C, copyright (c) American Chemical Society after peer review and technical editing by the publisher. To access the final edited and published work see https://doi.org/10.1021/acs.jpcc.3c03251.
Description	

Hole detrapping type persistent phosphors of RE_2O_2S (RE= La, Gd, Y, Lu) doped with Eu^{3+}-Pr^{3+} and Eu^{3+}-Tb^{3+}

*Atsunori Hashimoto[1, 2]‡, Jumpei Ueda[1,3 *]‡, Yasushi Aoki[2], Pieter Dorenbos[4], Setsuhisa Tanabe[3]*

[1] Graduate School of Advanced Science and Technology, Japan Advanced Institute of Science and Technology, 1-1 Asahidai, Nomi, 923-1292 Ishikawa, Japan

[2] NEMOTO & CO., LTD, 4-1 Shinmachi, Hiratsuka, 254-0076 Kanagawa, Japan

[3] Graduate School of Human and Environmental Studies, Kyoto University, 606-8501 Kyoto, Japan

[4] Faculty of Applied Sciences, Delft University of Technology, Mekelweg 15, 2629 JB Delft, The Netherlands

persistent phosphors, lanthanide ions, Hole trap, Eu^{3+}

ABSTRACT

RE$_2$O$_2$S:Eu^{3+}-*Ln*$^{3+}$ (*RE*=La, Gd, Y, Lu; *Ln*=Pr, Tb) samples were prepared by a solid-state reaction method to develop new red persistent phosphors and to demonstrate the hole de-trapping mechanism. All Eu^{3+}-singly doped *RE*$_2$O$_2$S show very weak thermoluminescence (TL) glow peaks, while by co-doping Pr^{3+} or Tb^{3+} ions additional strong TL peaks were observed. In the TL spectra and persistent luminescence (PersL) spectra, only Eu^{3+} luminescence lines were observed, but there is no Pr^{3+} and Tb^{3+} luminescence. From the PersL excitation spectra, it is found that the PersL is caused after the excitation to the charge transfer state of Eu^{2+}-S^{-} in which the hole is in the valence band. These results show that the Eu^{3+} acts as a recombination center and the Pr^{3+} and Tb^{3+} ion act as a hole trap center. The deeper hole trap depth of Pr^{3+} compared with Tb^{3+} and the *RE* dependence of hole trap depth are explained using a vacuum referred binding energy diagram considering the nephelauxetic effect. The La$_2$O$_2$S:Eu^{3+}-Pr^{3+} was the best composition among the samples as a persistent phosphor at the ambient temperature, showing the strong red persistent luminescence in a short time range (>100 mcd/m^2 for a few seconds).

1. Introduction

Persistent phosphors, which show continuing luminescence even after the ceasing of excitation light, have been widely used as luminous paint in many products such as an emergency sign, a dial plate of a watch, etc[1, 2]. In 1993, Nemoto company developed the brightest and longest green persistent phosphor, $SrAl_2O_4:Eu^{2+}$-Dy^{3+}, and published a paper in 1996 [3]. In this phosphor, the persistent luminescence is caused by the $4f^65d^1 \rightarrow 4f^7$ transition of Eu^{2+}. At that time, the persistent luminescence mechanism was not well understood and a hole transfer model (Eu^{2+}-$Dy^{3+} \Leftrightarrow Eu^{+}$-$Dy^{4+}$) was proposed. Nowadays, it is considered that the persistent luminescence in $SrAl_2O_4:Eu^{2+}$-Dy^{3+} is caused by the electron transfer process (Eu^{2+}-$Dy^{3+} \Leftrightarrow Eu^{3+}$-$Dy^{2+}$)[4, 5].

On the other hand, Nichia company successfully developed a bright red persistent phosphor, $Y_2O_2S:Eu^{3+}$-Ti^{4+}-Mg^{2+} in 1998[6]. The persistent luminescence center is Eu^{3+} which shows a strong red 4f-4f luminescence ($^5D_0 \rightarrow {}^7F_2$). Opposite to $SrAl_2O_4:Eu^{2+}$-Dy^{3+}, it is suggested that the $Y_2O_2S:Eu^{3+}$-Ti^{4+}-Mg^{2+} persistent luminescence is caused by the hole transfer process ($Eu^{3+} \Leftrightarrow Eu^{2+} + h^{+}$) although the hole trapping center is not identified[7]. To develop a new persistent phosphor based on the hole transfer model and to demonstrate its persistent luminescence mechanism in Eu^{3+}-doped rare earth oxysulfide compounds, the hole traps and their trap depth must be managed. The vacuum referred binding energy (VRBE) diagram of RE_2O_2S (*RE*=La, Gd, Y, Lu), demonstrates a possibility that Pr^{3+} and Tb^{3+} can act as a hole trap[7]. If the Pr^{3+} and Tb^{3+} ions act as traps in $RE_2O_2S:Eu^{3+}$ red phosphor, the mechanism of persistent luminescence is supported to be based on the hole transfer model. In the hole transfer model, the hole trap depth can be engineered by either selecting Pr^{3+} or Tb^{3+} or by altering the top of valence band energy

by changing the type of host compound rare earth ion. Also, recently, strong mechanoluminescence was reported in $RE_2O_2S:Ln^{3+}$ (RE = Y, Lu, La, or Gd; Ln = Eu, Pr, Nd, Sm, Tb, Dy, Ho, Er, Tm, or Yb)[8]. Thus, it is important to investigate carrier trapping and detrapping in $RE_2O_2S:Ln^{3+}$.

In this study, Eu^{3+}-Ln^{3+} (Ln = Pr and Tb) codoped RE_2O_2S (RE=La, Gd, Y, Lu) red persistent phosphors were prepared and its optical properties were investigated. From the results of thermoluminescence and persistent luminescence measurements, it is successfully demonstrated that the Pr^{3+} and Tb^{3+} ions act as hole traps. Also, variations in hole trap depths by Pr^{3+} and Tb^{3+} ions in RE_2O_2S host were explained using a newly constructed vacuum referred binding energy diagram that takes the nephelauxetic effect into account.

2. Experimental Procedure

$RE_{1.99}Eu_{0.01}O_2S$ and $RE_{1.988}Eu_{0.01}Ln_{0.002}O_2S$ (RE=La, Gd, Y, Lu; Ln=Pr, Tb) were prepared by a solid state reaction method. La_2O_3, Gd_2O_3, Y_2O_3, Lu_2O_3, Eu_2O_3, Pr_6O_{11}, Tb_4O_7, S were used as raw materials. In order to prevent oxidation, an excess amount of sulfur was added. Also, Na_2CO_3 and K_3PO_4 were used to facilitate the solid-state reaction. These chemicals were mixed by ball milling and sintered at 1200°C for 4 h in air. The obtained materials were washed by deionized water several times to remove remnants. The crystal phases of samples were analyzed by an XRD measurement system (XRD-6100, Shimadzu). Photoluminescence (PL) and photoluminescence excitation (PLE) spectra were measured by a self-built spectrometer; monochromatic excitation light was generated by a 500 W Xe short arc lamp (OPM2-502XQ, Ushio Inc.) and a double monochromator setup using two single monochromators (SpectraPro-

300i, Acton Research Corporation) and luminescence was detected by a photomultiplier tube (R10699, Hamamatsu Photonics) equipped with a single monochromator (SP-2300i, Princeton Instruments). The measured PLE spectra were calibrated by a photon flux spectrum of excitation light source which is measured using a standard Si (S1337-1010BQ, Hamamatsu Photonics). The PL spectra were calibrated by a standard halogen lamp (DH-2000CAL, Ocean Photonics) to the photon flux spectrum. Thermoluminescence (TL) glow curves were measured using a photomultiplier tube, PMT (R3896, Hamamatsu Photonics) with a bandpass filter of 640 nm with 100 nm FWHM. The samples were fixed into cryostat (VPF-800, Janis) to control the temperature. The samples were charged by UV excitation (250 ~ 400 nm) from a 300 W Xe-lamp (MAX-302, Asahi Spectra) at 80 K for 10 min and kept for 10 min after ceasing excitation at the same temperature. The sample was then heated with the heating rate of 10 K/min up to 400 K. The TL spectra were measured simultaneously by a Si CCD spectrometer (QE65-Pro, Ocean Optics). Persistent luminescence (PersL) spectra were detected by a Si CCD spectrometer (PMA-12, Hamamatsu Photonics). PersL decay curves were measured by the luminance meter (LS-100, KONICA MINOLTA) after UV irradiation. For PersL excitation (PersLE) spectra, the sample was irradiated for 5 min by the monochromatic light and 1 min after stopping irradiation PersL spectra were measured by the spectrophotometer (RF-5000, Shimadzu).

3. Results

3.1. Crystal structure

Figure 1 shows the X-ray diffraction (XRD) patterns of Eu^{3+} doped RE_2O_2S ($RE_2O_2S:Eu^{3+}$; *RE*=La, Gd, Y, Lu). The observed XRD patterns of Eu^{3+}-doped La_2O_2S, Gd_2O_2S, Y_2O_2S and Lu_2O_2S correspond to the reference XRD patterns of RE_2O_2S (*RE*=La, Gd, Y, Lu) in the ICDD

(International Centre for Diffraction Data) database with the card number #01-071-2098, #01-079-5662, #00-024-1424 and #00-026-1445, respectively. Thus, all samples are identified as a single crystalline phase of RE_2O_2S (RE=La, Gd, Y, Lu) with the space group of $P\bar{3}m1$. The observed XRD peaks are shifted to the higher diffraction angle in the order of La_2O_2S, Gd_2O_2S, Y_2O_2S and Lu_2O_2S because the cation size of RE ion becomes smaller in the same order. Consequently, the lattice constant decreases in the order of La_2O_2S, Gd_2O_2S, Y_2O_2S and Lu_2O_2S.

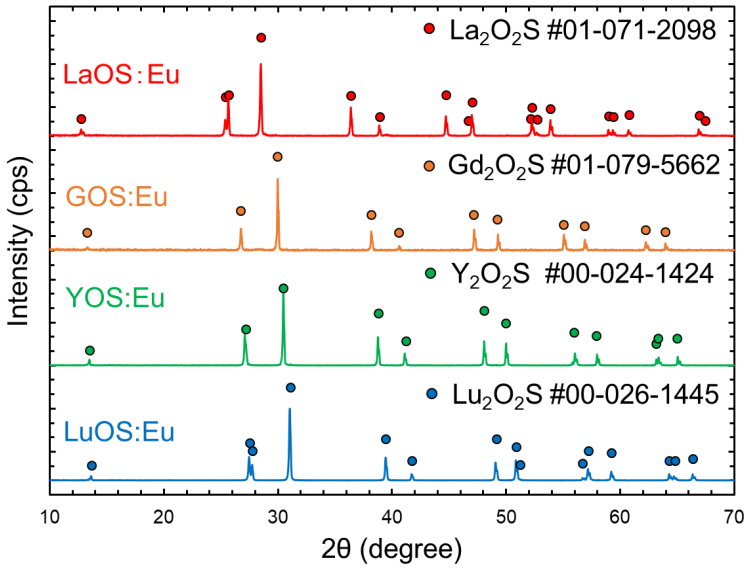

Figure 1. X-ray diffraction (XRD) patterns of the $RE_2O_2S:Eu^{3+}$ (RE = La, Gd, Y, Lu).

3.2. PL and PLE properties

Figure 2 shows the PL spectra of $RE_2O_2S:Eu^{3+}$ (RE=La, Gd, Y, Lu). All samples show strong red luminescence mainly due to the typical Eu^{3+} 4f-4f luminescence ($^5D_0 \rightarrow {}^7F_2$) at around 625 nm. The peak wavelength of the $^5D_0 \rightarrow {}^7F_2$ in La_2O_2S, Gd_2O_2S, Y_2O_2S and Lu_2O_2S were 624.6nm, 626.4nm, 627.0nm, 627.6nm, respectively, at ambient temperature. In addition to the $^5D_0$-^7F_J

luminescence lines from 590 nm to 720 nm, several PL peaks were observed in the range from 450 nm to 575 nm in the Gd_2O_2S, Y_2O_2S and Lu_2O_2S samples. On the other hand, for $La_2O_2S:Eu^{3+}$, the luminescence peaks in the range from 450 nm to 520 nm are almost quenched at ambient temperature. These PL peaks can be attributed to the $^5D_1 - ^7F_J$ and $^5D_2 - ^7F_J$ luminescence as shown in Figure 2.

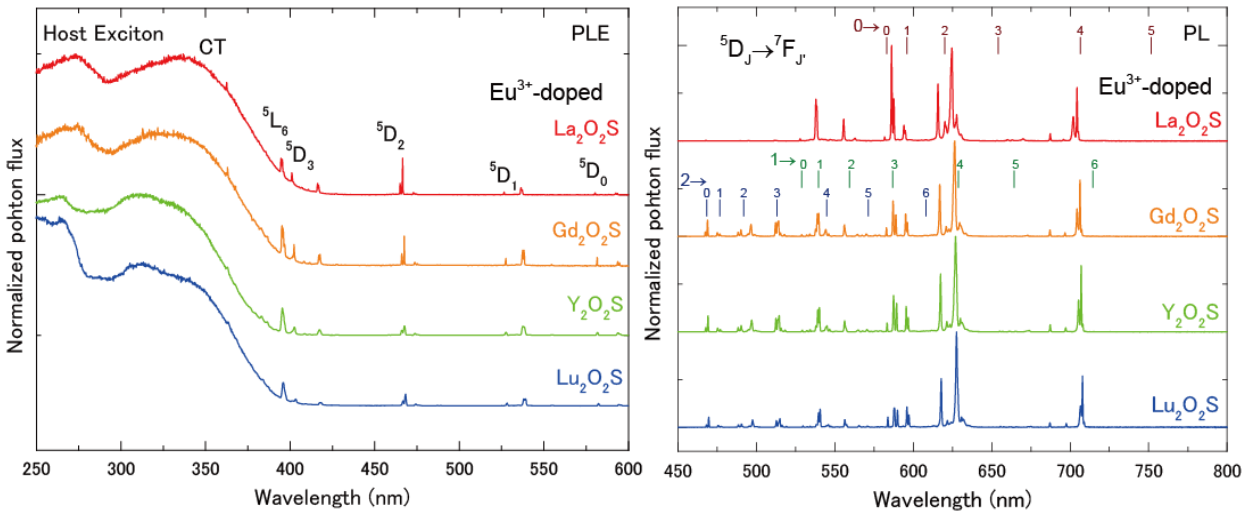

Figure 2. (a) PLE and (b) PL spectra at room temperature of the RE2O2S: Eu3+ (RE = La, Gd, Y, Lu).

In the PLE spectra, sharp lines at around 395 nm, 470 nm, 530 nm and 580 nm and two broad bands in the range between 250 nm and 290 nm and between 290 nm and 400 nm were observed. The sharp lines are attributed to 4f-4f transitions of Eu^{3+} from $^7F_0$ to $^5L_6$, $^5D_2$, $^5D_1$ and $^5D_0$. The broad band in the longer wavelength range originates from electron transfer from the valence band to Eu^{3+}, which is called the charge transfer (CT) band. The broad band in the shorter wavelength at around 270 nm originates from the host exciton creation bands. The energy of the CT band and the host exciton band varied by depending rare earth ion of the host compound. To clarify the host exciton energy and the CT energy in each host compound, the PLE spectra from

the VUV to UV were also measured at 15 K (see Figure S1 in the supporting information). The host exciton energy is shifted to higher energy in the order of La_2O_2S (4.62 eV), Gd_2O_2S (4.66 eV), Y_2O_2S (4.81 eV) and Lu_2O_2S (5.19 eV). The exciton creation energy seems to be very high only for the $Lu_2O_2S:Eu^{3+}$ although the exciton creation energy of $Lu_2O_2S:Eu^{3+}$ at room temperature is similar to other RE_2O_2S compounds (Figure 2). Compared with the PLE spectra of $Lu_2O_2S:Eu^{3+}$ in VUV region at 300 K and 15 K (Figure S2), the spectral shape is dramatically changed. Because the Lu_2O_2S is a mixed anion compound, the host exciton absorption may occur from oxide 2p and sulfide 3p orbitals. At 15K the energy transfer from the exciton absorption due to the S(3p)-Lu(5d) to Eu^{3+} may not take place efficiently in $Lu_2O_2S:Eu^{3+}$(Figure S2). Consequently, the host excitation energy at 15K was overestimated in Lu_2O_2S. Thus, the host exciton energy of 4.82 eV, which was estimated from the exciton peak at room temperature with a correction of 0.15 eV by temperature effect, was used only for Lu_2O_2S.

3.3. TL and PersL properties

Figure 3 shows TL glow curves of $La_2O_2S:Eu^{3+}$ and $La_2O_2S:Eu^{3+}$-Ln^{3+} (*Ln*=Pr, Tb). By co-doping with Pr^{3+} and with Tb^{3+}, additional strong TL peaks were observed. The TL peak temperature of $La_2O_2S:Eu^{3+}$-Pr^{3+} and $La_2O_2S:Eu^{3+}$-Tb^{3+} are 242 K and 233 K, respectively. The additional TL peaks by co-doping with Pr^{3+} and with Tb^{3+} were also observed in other RE_2O_2S hosts (See Figure S3, S4 and S5 in the supporting information). The TL glow curves in $RE_2O_2S:Eu^{3+}$-Ln^{3+} (*RE*=La, Gd, Y, Lu; *Ln*=Pr, Tb) are summarized in the series of Pr^{3+} codopant and Tb^{3+} codopant as shown in Figure 4a and 4b, respectively. The TL glow peak is shifted by varying the rare earth ion of host compounds. The main TL glow peak temperature in La_2O_2S is the highest, followed by Y_2O_2S, Gd_2O_2S, Lu_2O_2S in both series of $RE_2O_2S:Eu^{3+}$-Pr^{3+} and $RE_2O_2S:Eu^{3+}$-Tb^{3+}. The TL glow peak temperatures for $RE_2O_2S:Eu^{3+}$-Ln^{3+} (*RE*=La, Gd, Y, Lu;

Ln=Pr, Tb) are listed in Table 1. When we compare the original TL glow peak intensity, the La_2O_2S and Y_2O_2S hosts show better performance than Gd_2O_2S and Lu_2O_2S both in Pr^{3+}-codoped ones and Tb^{3+}-codoped ones (See Figure3 and Figure S3, S4 and S5 in the supporting information) .

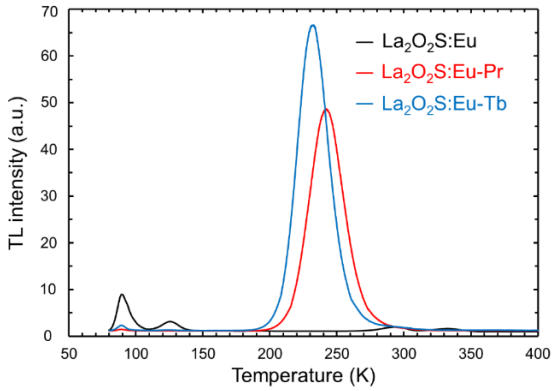

Figure 3. TL glow curves of the $La_2O_2S:Eu^{3+}$, $La_2O_2S:Eu^{3+}$-Ln^{3+} (*Ln* = Pr, Tb) at heating rate of 10 K/min after UV (250~400 nm) irradiation for 10 min.

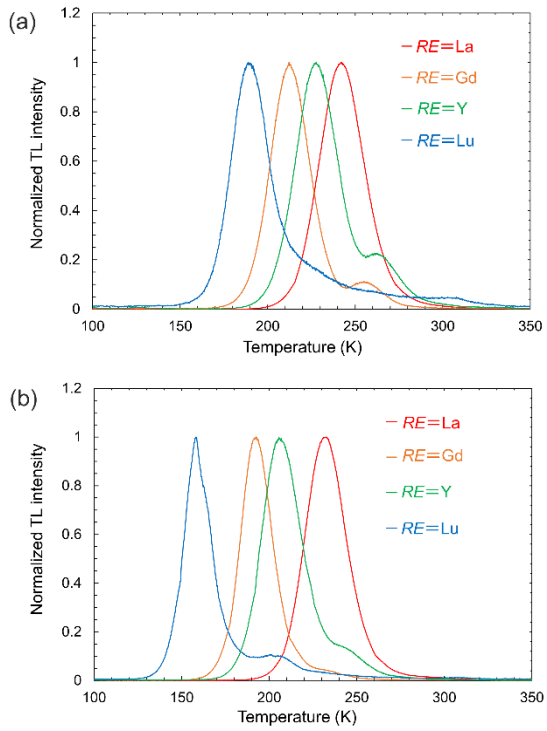

Figure 4. TL glow curves of the $RE_2O_2S:Eu^{3+}$ (*RE*=La, Gd, Y, Lu) (a) with Pr^{3+} codopant and (b) with Tb^{3+} codopant at heating rate of 10 K/min after UV (250~400 nm) irradiation for 10 min.

Table 1. Frequency factor (s)[7], temperature maximum (T_m) of TL glow curves at heating rate of 10 K/min and the derived trap depth (E^{trap}) of $RE_2O_2S:Eu^{3+}$-Ln^{3+} (*RE*=La, Gd, Y, Lu, *Ln*=Pr, Tb).

		T_m (K)		E^{trap} (eV)	
	Frequency factor (s^{-1}) [7]	Pr	Tb	Pr	Tb
RE = La	1.1×10^{13}	242	233	0.70	0.68
RE = Gd	1.3×10^{13}	212	192	0.62	0.56
RE = Y	1.3×10^{13}	228	206	0.66	0.60
RE = Lu	1.4×10^{13}	189	158	0.55	0.46

From the well-known equation for the TL glow curve caused by first-order kinetics carrier transportation as presented by Randall and Wilkins,[9, 10] one can derive[11]

$$\frac{\beta E^{trap}}{kT_m{}^2} = s \cdot exp\left(-\frac{E^{trap}}{kT_m}\right) \qquad (1).$$

Here, β is the heating rate (K/s), E^{trap} is trap depth, k is the Boltzmann constant, T_m is the maximum temperature of TL glow peak, s is the frequency factor. Thus, from the obtained TL glow peak temperature, the trap depths can be estimated by assuming the frequency factor. The frequency factors were reported in the reference[7] as shown in column 2 of Table 1. The calculated trap depths in the $RE_2O_2S:Eu^{3+}$-Ln^{3+} (RE=La, Gd, Y, Lu; Ln=Pr, Tb) are shown in Table 1. The trap depth of main peak TL glow peak in RE = La is the deepest, followed by RE= Y, Gd and Lu both in the series of $RE_2O_2S:Eu^{3+}$-Pr^{3+} and $RE_2O_2S:Eu^{3+}$-Tb^{3+}.

Figure 5 shows the luminescence wavelength-temperature (λ_{em}-T) contour plots of TL intensity of the $La_2O_2S:Eu^{3+}$-Ln^{3+} (Ln=Pr, Tb). The observed TL peaks originate only from Eu^{3+} 4f-4f transition. No TL emission from Pr^{3+} and Tb^{3+} were observed in the temperature range from 100 K to 400 K.

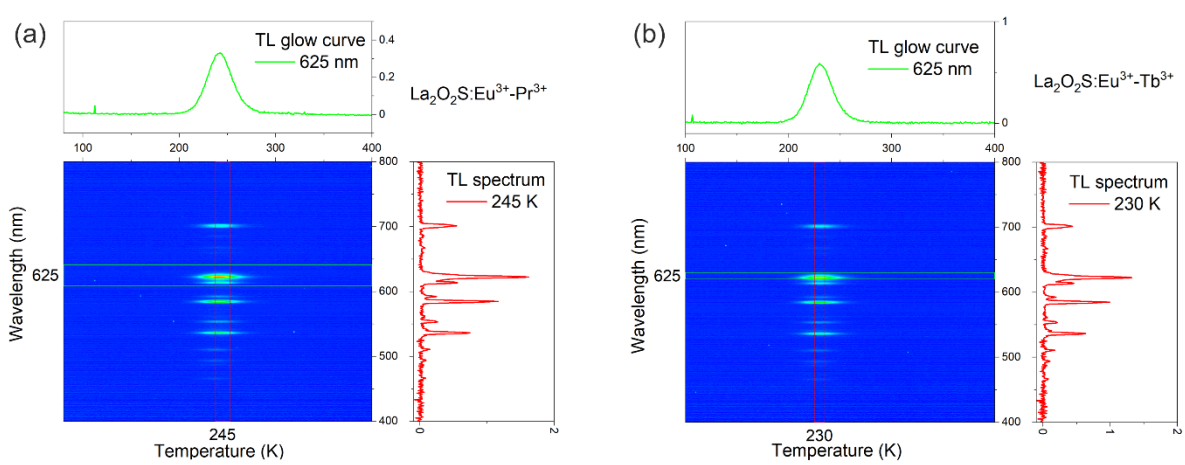

Figure 5. Emission wavelength-temperature (λ_{em}-T) contour plots of TL intensity for (a) $La_2O_2S:Eu^{3+}$-Pr^{3+} and (b) $La_2O_2S:Eu^{3+}$-Tb^{3+}

Figure 6a shows PersL spectra of $La_2O_2S:Eu^{3+}$and $La_2O_2S:Eu^{3+}$-Ln^{3+} (*Ln* = Pr, Tb). These samples showed red persistent luminescence. By co-doping the lanthanide ions, the intensities of persistent luminescence become stronger compared with Eu^{3+} singly-doped La_2O_2S. In these samples, no persistent luminescence from Pr^{3+} and Tb^{3+} was observed similar to TL spectra in Figure 5 which indicates that only the Eu^{3+} ions act as a recombination center. In the samples of *RE* = Gd, Y, and Lu, the PersL cannot be detected by the Si CCD at ambient temperature because of the too shallow trap depths. Figure 6b shows the PersL decay curves of the $La_2O_2S:Eu^{3+}$and $La_2O_2S:Eu^{3+}$-Ln^{3+} (*Ln* = Pr, Tb) samples. By the addition of the co-dopant, the luminance is enhanced compared with Eu-singly doped La_2O_2S. Persistent luminescence duration of $La_2O_2S:Eu^{3+}$-Pr^{3+} is the longest in these La_2O_2S-based samples and the duration time is 60s until the luminance drops 2 mcd/m^2.

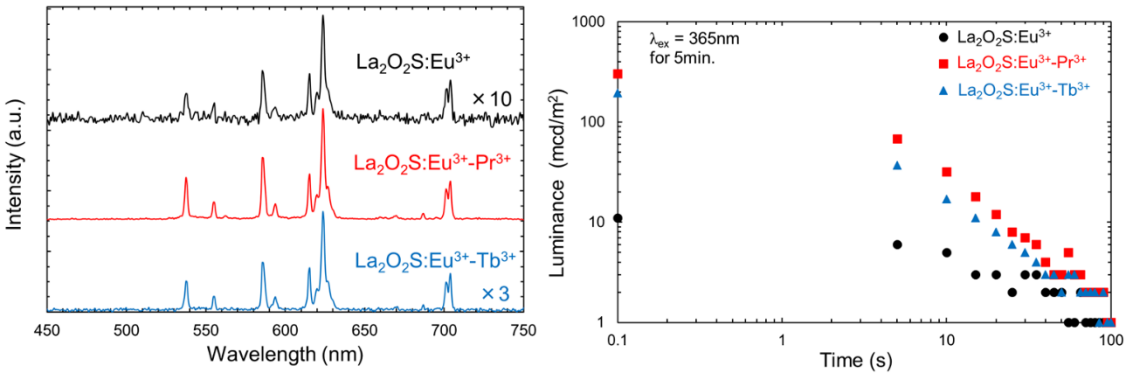

Figure 6. (a) PersL spectra and (b) PersL decay curves of $La_2O_2S:Eu^{3+}$and $La_2O_2S:Eu^{3+}$-Ln^{3+} (*Ln* = Pr, Tb).

Figure 7 shows the PersLE spectra of $La_2O_2S:Eu^{3+}$-Pr^{3+}. Two excitation bands were observed; The PersLE band at 230 nm is attributed to the host exciton creation band and another band at 380 nm is the CT band of Eu^{3+}.

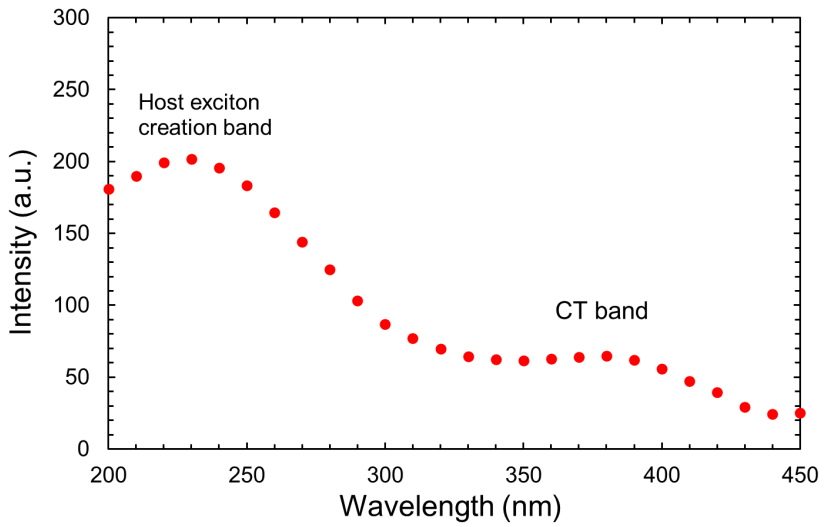

Figure 7. PersL excitation spectra of $La_2O_2S:Eu^{3+}$-Pr^{3+}

4. Discussion

4.1. Quenching process and Nephelauxetic effect of Eu^{3+} luminescence

As shown in Figure 2b, only La_2O_2S does not show the luminescence from $^5D_2$ excited state. The possible quenching processes are multiphonon relaxation, cross-relaxation and the thermally activated crossover to the CT state. The relatively low phonon energies (~500 cm^{-1})[12] of the RE_2O_2S compounds imply no multiphonon relaxation quenching. Also, the low Eu^{3+} concentration (0.5 %) means no cross-relation quenching. However, the CT absorption edge of $La_2O_2S:Eu^{3+}$ in Fig. 2a shows the longest wavelength among the $RE_2O_2S:Eu^{3+}$ (RE=La, Gd, Y and Lu), indicating that the activation energy to the CT state

is small. Thus, the $^5D_2$ luminescence quenching in $La_2O_2S:Eu^{3+}$ can be caused through the CT state.

4.2. Hole trap by Pr^{3+} and Tb^{3+}

As expected, the Pr^{3+} and Tb^{3+} co-doping generated additional TL glow peaks (Figure 3, 4). The persistent luminescence (thermoluminescence) center was identified to be only Eu^{3+} based on the PersL and TL spectra (Figure 5, 6). The Eu^{3+} persistent luminescence was caused after excitation upon the charge transfer band of Eu^{3+} and band-to-band absorption (Figure 7). These results strongly show that the persistent luminescence is caused by the hole transfer process.

When the CT band of Eu^{3+} is excited, the Eu^{3+}-S^{2-} state is changed into Eu^{2+}-S^{-} because the electron of 3p orbital of S^{2-} is transferred to Eu^{3+}. One may equally well state that a hole is transferred from Eu^{3+} to S^{2-} which forms the top of VB. In the hole picture model [13], the CT excitation is depicted by arrow 1 in Figure 8. This free hole in the valence band can be captured by Ln^{3+} (Pr^{3+}, Tb^{3+}), which then changes into a tetravalent state. The tetravalent state is known as a stable valence state for Pr and Tb in many compounds. This hole trapping process is illustrated by arrow 2 in Figure 8. On the other hand, the Eu^{3+} ion keeps the excited electron from S^{2-} through the CT absorption, which means that the Eu^{3+} ion acts as an electron trap. Thus, the valence state changing of Eu^{3+}-Ln^{3+}⇔Eu^{2+}- Ln^{4+} (Ln= Pr, Tb) is our proposed carrier trapping mechanism. So far, these kinds of valence state changing have been demonstrated using UV-Vis absorption spectroscopy and X-ray absorption spectroscopy[5, 14-17]. The trapped hole by Pr^{3+} or Tb^{3+} can be released at a lower temperature than the electron from the electron-trapped-Eu^{3+} (Eu^{2+}). If the electron of Eu^{2+} is de-trapped at a lower temperature, the Pr^{3+} and Tb^{3+} ions should be recombination centers, but the PersL of Pr^{3+} and Tb^{3+} was not observed. Thus, the

hole transfer and the hole de-trapping process support the fact that only Eu^{3+} shows persistent luminescence.

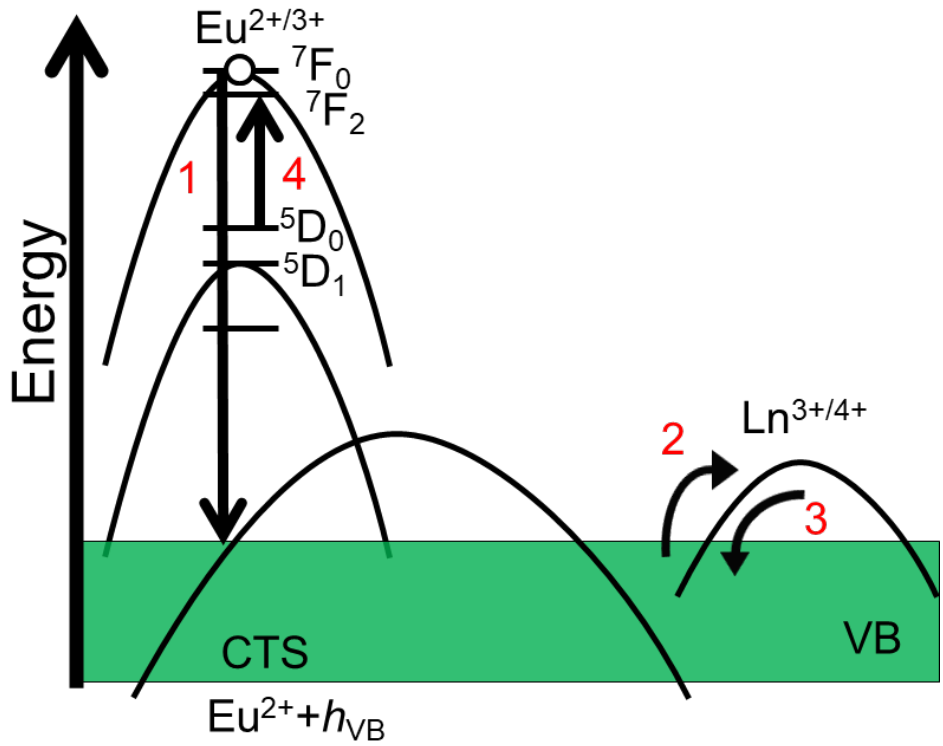

Figure 8. Persistent luminescence mechanism based on the hole picture model. 1. Excitation to charge transfer state, 2. hole trapping, 3. hole detrapping, 4. $^5D_0$-$^7F_2$ luminescence.

4.3. Hole trap depth in VRBE diagram

To understand the hole trap depth by Pr^{3+} and Tb^{3+} in RE_2O_2S, the VRBE (vacuum referred binding energy diagram) can be useful. The VRBE diagrams of RE_2O_2S were reported by Hongde et al. in 2017. Based on the VRBE in 2017, it is considered that the Tb^{3+} forms deeper

hole traps compared with Pr^{3+} in all the RE_2O_2S hosts and the hole trap depth of both Pr^{3+} and Tb^{3+} becomes deeper in the order of La_2O_2S, Gd_2O_2S, Y_2O_2S and Lu_2O_2S with decreasing *RE* ionic radius as shown in Table 2. However, the obtained trap depth in the $RE_2O_2S:Eu^{3+}$-Ln^{3+} as shown in Table 1 does not follow this trend. The observed hole trap depth of Tb^{3+} is always shallower than that of Pr^{3+} in all the RE_2O_2S hosts. In addition, the hole trap depth by Pr^{3+} and Tb^{3+} in La_2O_2S is the deepest and that in Lu_2O_2S is the shallowest among the RE_2O_2S hosts.

Table 2. Estimated hole trap depth of Pr^{3+} and Tb^{3+} in RE_2O_2S hosts based on the VRBE diagram reported in reference[7] in eV.

	Pr^{3+}	Tb^{3+}
La_2O_2S	0.63	0.81
Gd_2O_2S	0.74	0.92
Y_2O_2S	0.77	0.95
Lu_2O_2S	0.79	0.97

Although the typical errors in VRBE construction are several 0.1 eV, there seems to be a clear inconsistency in the trends with changing RE and between Pr^{3+} and Tb^{3+}. In 2019, Dorenbos improved the model of VRBE diagram construction by considering the Nephelauxetic effect on VRBE energies[18]. It was found that the nephelauxetic effect may lower the right hand branch (n=8 to 14) of the zig-zag curves of Ln^{2+} and Ln^{3+} by several 0.1 eV with respect to the left hand branch (n=1 to 7). Here, *n* is the number of 4f electrons of Ln^{3+}. In the RE_2O_2S hosts, an enhanced nephelauxetic effect is to be expected due to the smaller electronegativity of sulfide (χ_S=2.58) compared with pure oxide materials (χ_O=3.44). The branch lowering in the zig-zag curve of Ln^{3+} is crucial for the hole trap depth difference between Pr^{3+} and Tb^{3+}[19]. For instance, in the $REPO_4$

compounds which show a low nephelauxetic effect by oxygen ligand because of the strong bonding between P^{5+} and O^{2-}, the Tb^{3+} hole trap depth is deeper than the Pr^{3+} hole trap. On the other hand, in the rare earth aluminates such as $Y_3Al_5O_{12}$ and $GdAlO_3$ which show a slightly larger nephelauxetic effect due to the weaker bonding of Al^{3+}-O^{2-} than P^{5+}-O^{2-}, the Tb^{3+} hole trap depth is shallower than the Pr^{3+} hole trap[19]. The same appears now for the oxysulfides in this work. Dorenbos introduced the nephelauxetic ratio β as a parameter to quantify the branch lowering [18, 19]. β is defined by the ratio of Slater-Condon parameter F^2 for the lanthanides in a compound A with respect to that for lanthanides in vacuum. The β parameter is directly linked to the energy difference ΔE(8,2,A) between the VRBE of Tb^{3+} and the VRBE of Pr^{3+} [19]. From the hole trap depths (Table 1), the ΔE(8,2,A) of La_2O_2S, Gd_2O_2S, Y_2O_2S and Lu_2O_2S amount -0.02, -0.06, -0.06 and -0.09 eV, respectively, which leads into the decreasing β parameter as like 0.930, 0.927, 0.927 and 0.924. The decreasing tendency of β in the order of La_2O_2S, Gd_2O_2S, Y_2O_2S and Lu_2O_2S suggests that the environment at the RE-site becomes more covalent. This tendency cannot be explained by the electronegativity of RE-cation which increases from La to Lu. In this series, smaller RE-site size can increase the nephelauxetic effect due to the shorter distance with anion.

Also, the same nephelauxetic effect is apparent in the Eu^{3+} luminescence peak position. Figure 9 shows host rare earth ion dependence of the Eu^{3+}:$^5D_0$-$^7F_0$ energy in RE_2O_2S obtained from PL spectra in Figure 2 together with data on RE_2O_3:Eu^{3+} as a reference. For the RE_2O_3:Eu^{3+} series, the Eu^{3+}:$^5D_0$-$^7F_0$ energies at the C_2 site of C-type RE_2O_3 for RE=Gd, Y, Lu[20] and at the C_{3v} site of A-type La_2O_3[21] are shown. The Eu^{3+}:$^5D_0$-$^7F_0$ energy shifts to lower energy with decreasing RE ionic radius in the RE_2O_2S hosts, whereas for RE_2O_3:Eu^{3+} the energy remains fairly constant. Generally, the 4f-4f transition energy can be affected by both the crystal field [22, 23] and the nephelauxetic effect [24-26]. Because the Eu^{3+}:$^5D_0$-$^7F_0$ does not show any luminescence lines related to the Stark

splitting, the Eu^{3+}:$^5D_0$-$^7F_0$ reflects only nepheraluxetic effect. Also, in the series of RE_2O_2S with the same crystal structure, the Eu^{3+} luminescence energy can be shifted to lower energy mainly by enhancing the nephelauxetic effect. This is probably because of the unique crystal structure of RE_2O_2S and the small electronegativity of S^{2-}. The RE_2O_2S crystal forms a layered structure by S^{2-}, O^{2-} and RE^{3+} sheets and the *RE* site is asymmetrically coordinated by four O^{2-} and three S^{2-} as shown in Figure 10. For this asymmetric coordination, the 4f electron cloud can be expanded to the S^{2-} ions because of the smaller electronegativity than oxide (χ_S=2.58 < χ_O=3.44). These unique crystal structure and smaller RE site may lead into the increase of nephelauxetic effect. This strong nephelauxetic effect for Eu^{3+} applies equally well to all other Ln^{3+} ions. From the host compound dependence of the hole trap difference between Pr^{3+} and Tb^{3+} and the Eu^{3+} luminescence red-shifting, the decreasing β parameter in the order of La_2O_2S, Gd_2O_2S, Y_2O_2S and Lu_2O_2S appears consistent and reasonable.

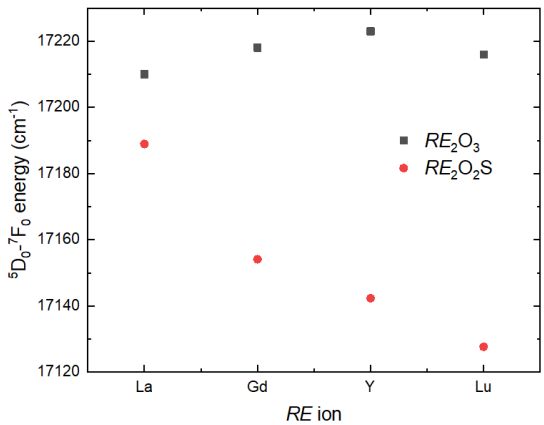

Figure 9. Host rare earth ion dependence of Eu^{3+}:$^5D_0$-$^7F_0$ energy in RE_2O_2S and RE_2O_3 [20, 21].

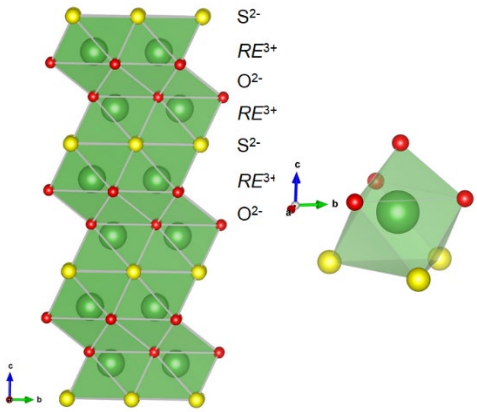

Figure 10. Crystal structure of RE_2O_2S. (The crystal structure is drawn by VESTA software.[27])

4.4. Construction of VRBE diagram considering the nephelauxetic effect

Based on the observed trap depth variation of Pr^{3+} and Tb^{3+} in RE_2O_2S, new VRBE diagrams that take the nephelauxetic effect into account need to be constructed. To make a new VRBE diagram, the required energetic parameters were also updated based on the newly obtained spectroscopic data. They are compiled in Table 3. The exciton creation energy was determined from the PLE from the VUV to UV range at 15 K (Figure S1 in the supporting information) as treated in section 3.2. To obtain the CT energies, the PLE spectra in the energy scale from Figure 2 were deconvoluted by two Gaussian peaks because we assumed CT absorption both from O^{2-} and from S^{2-}. For example, two clear PLE bands can be seen in Fig. 2a for $Lu_2O_2S:Eu^{3+}$. The electronegativity of S is smaller than that of O, forming the top of valence state by 3p orbital of S. Thus, the lower CT energies were used for the VRBE diagram. Red-shift parameter of Ce^{3+} was calculated using the 4f-5d$_1$ absorption peak reported in the reference [28]. The U(6, A) value of RE_2O_2S is reported to be around 6.37 eV [7]. U(6,A) is the energy

difference between the VRBE of Eu^{2+} and Eu^{3+} and it depends on the screening distance in the chemical shift model[29]. In this study, we also adopted a U(6,A) value of 6.37 eV.

Table 3. Parameters and spectroscopic data utilized to construct the VRBE diagram of *Ln* in the RE_2O_2S host and the estimated VRBE values in eV unit (except for Nephelauxetic ratio β). The method of the reference[12,13] was followed.

	U(6,A)	E^{ex}	E^{CT}	β	D(1,3+,A)	E_V	E_C	E_{Eu2+}	E_{Pr3+}	E_{Tb3+}
La_2O_2S	6.37	4.62	3.58	0.930	3.39	-7.34	-2.72	-3.77	-6.64	-6.67
Gd_2O_2S	6.37	4.66	3.60	0.927	3.45	-7.43	-2.77	-3.75	-6.57	-6.63
Y_2O_2S	6.37	4.81	3.58	0.927	3.44	-7.37	-2.56	-3.77	-6.63	-6.68
Lu_2O_2S	6.37	4.82	3.56	0.924	3.45	-7.34	-2.52	-3.78	-6.67	-6.75

U(6,A): energy difference between the VRBE of Eu^{2+} and Eu^{3+} in host A, E^{ex}: host exciton creatin energy, E^{CT}: charge transfer energy from anion to Eu^{3+}, β: Nephelauxetic ratio, D(1,3+,A): energy difference between the quasi free ion 4f–5d energy and the observed 4f–5d energy of Ce^{3+} in host A, $E_{V,C,\ Eu2+,\ Pr3+\ and\ Tb3+}$: VRBE of valence band top, conduction band bottom, Eu^{2+}, Pr^{3+} and Tb^{3+}, respectively.

Figure 11 shows the new VRBE diagram for La_2O_2S using the updated parameters. Different from the previous VRBE diagram, the VRBE of Tb^{3+} is located slightly below that of Pr^{3+}. The electron trap depth by Eu^{3+} is 1.21 eV and the hole trap depth by Pr^{3+} and Tb^{3+} are 0.78 and 0.75 eV, respectively. Because the hole trap depth by Pr^{3+} and Tb^{3+} is smaller than the electron trap depth by Eu^{3+}, the hole trap is released at lower temperature than the electron trap. Thus, the VRBE diagram also supports the hole-detrapping mechanisms for the persistent luminescence.

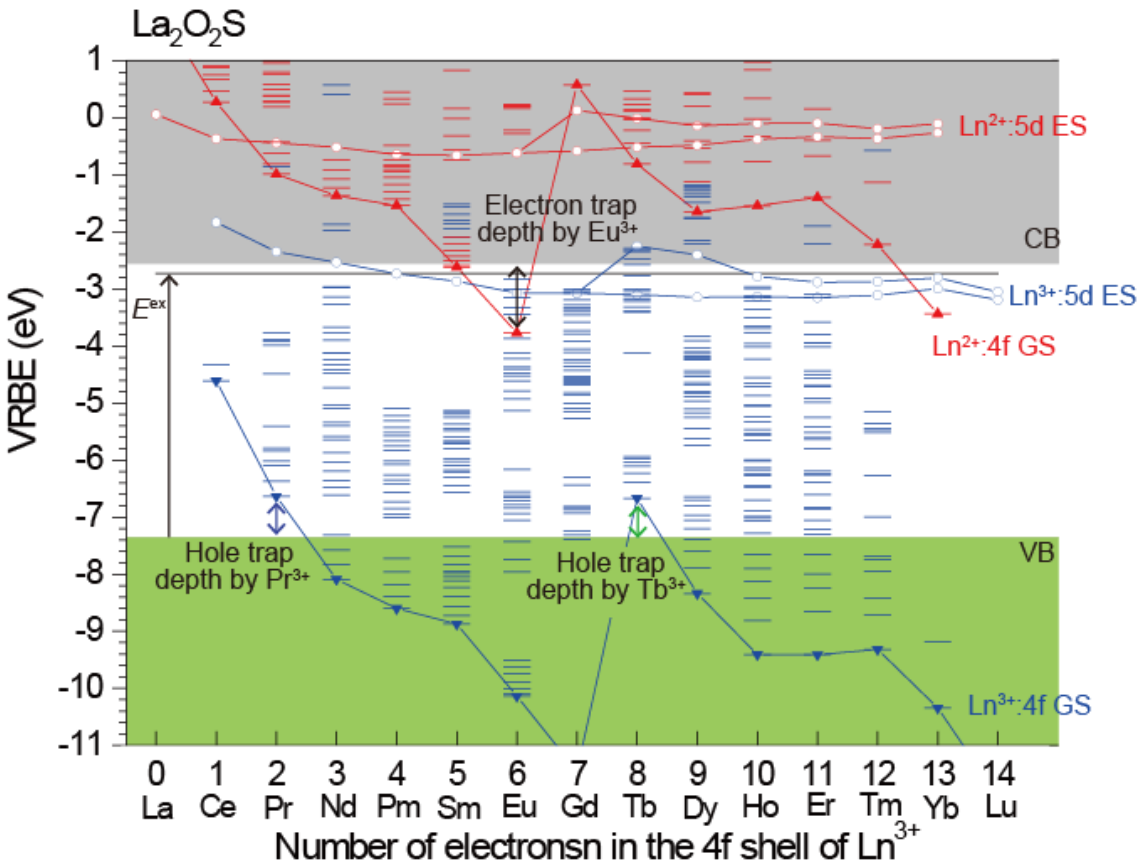

Figure 11. VRBE diagram of La_2O_2S. VB: valence band, CB: conduction band, GS: ground state, ES: Excited state, *Ln*: Lanthanide ions

Figure 12 shows a stacked VRBE diagram of RE_2O_2S. In the new VRBE diagram, the observed unusual trend of hole trap depth (the deepest in La_2O_2S and the shallowest in Lu_2O_2S) can be explained partly. The energy difference between the top of VB and Ln^{3+} (Pr^{3+}, Tb^{3+}) in La_2O_2S is much larger than that in Lu_2O_2S. Figure 13 summarizes the hole trap depth by Pr^{3+} and Tb^{3+} estimated from the experimental results and the VRBE diagram. The VRBE diagram cannot explain the hole trap depth in Gd_2O_2S while it can explain the decreasing trend of hole trap depth from La to Lu. For this trend, the La_2O_2S:Eu^{3+}-Ln^{3+} show the deep trap depth among the RE_2O_2S hosts and it is closest to ambient temperature. For the application demanding the

longer persistent duration, the $La_2O_2S:Eu^{3+}$-Ln^{3+} is not suitable. However, the strong red persistent luminance in a short time range (>100mcd/m^2 for a few seconds) for the $La_2O_2S:Eu^{3+}$-Pr^{3+} can be used as security ink and so on.

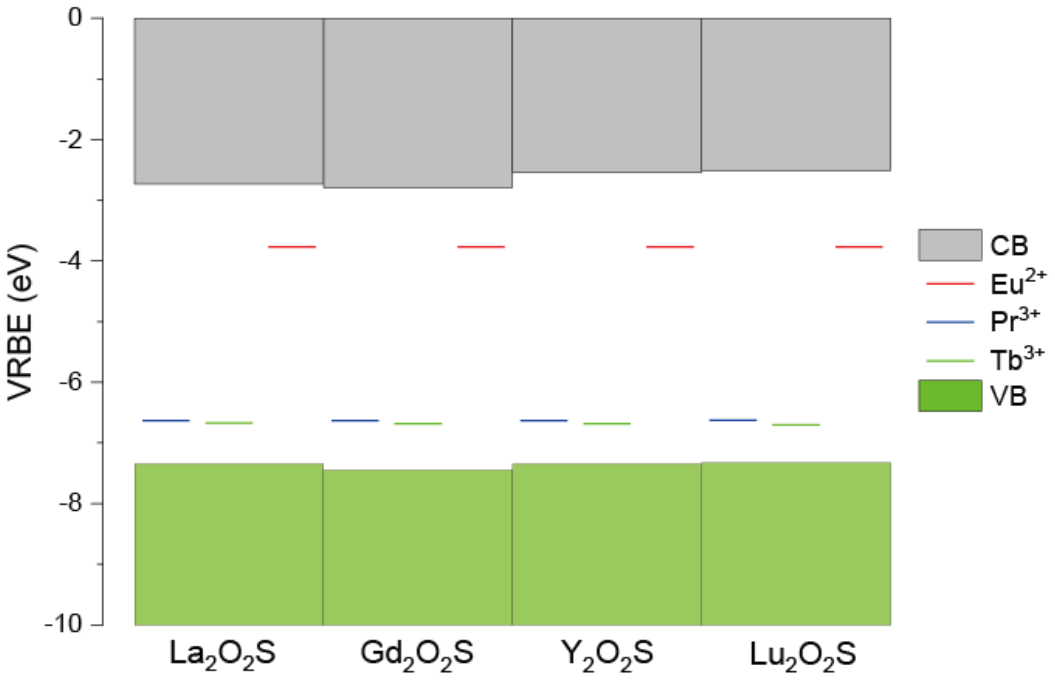

Figure 12. Stacked VRBE diagram of RE_2O_2S with ground state of Eu^{2+}, Pr^{3+} and Tb^{3+}.

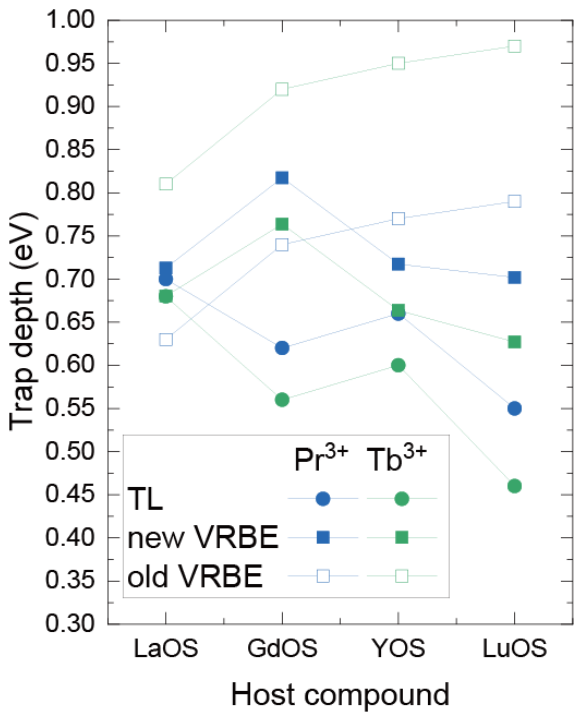

Figure13. Hole trap depths of Pr^{3+} and Tb^{3+} estimated from the TL glow peak and from the reported VRBE diagram[5] and the newly constructed VRBE diagram.

5. Conclusion

Red $RE_2O_2S:Eu^{3+}$-Ln^{3+} (*RE*=La, Gd, Y, Lu; *Ln*=Pr, Tb) thermoluminescence phosphors were developed, where Pr^{3+} and Tb^{3+} co-doping generated additional TL glow peaks. The persistent luminescence and thermoluminescence have been identified to arise from only Eu^{3+}. Eu^{3+} persistent luminescence appears after excitation in the charge transfer band of Eu^{3+} and by means of band-to-band excitation. Based on the obtained results, it was concluded that the persistent luminescence of Eu^{3+} is caused by the hole trapping at Pr^{3+} and Tb^{3+} followed by a thermally de-trapping process. The vacuum referred binding energy diagrams of RE_2O_2S taking into account the nephelauxetic effect was constructed. Using a new VRBE diagram, the deeper hole trap of

Pr^{3+} than that of Tb^{3+} was explained by a right hand branch lowering of the zig-zag curve of Ln^{3+} due to an enhanced nephelauxetic effect caused by the sulfide ions. This is consistent with an observed redshifting of the Eu^{3+} emission lines. The hole trap depth tendency of Pr^{3+} and Tb^{3+} with respect to different host of RE_2O_2S except Gd_2O_2S was understood by a new VRBE diagram. The $La_2O_2S:Eu^{3+}$-Pr^{3+} is among the samples the best composition for a persistent phosphor at ambient temperature, showing a strong red persistent luminescence in a short time range (>100 mcd/m^2 for a few seconds).

ASSOCIATED CONTENT

Supporting Information. The following files are available free of charge.

PLE in vacuum UV region, TL glow curves. (PDF)

AUTHOR INFORMATION

Corresponding Author

*E-mail: ueda-j@jaist.ac.jp

Author Contributions

JU conceived the idea of the study. AH and YA prepared the materials. JU and AH investigated the structure properties and optical properties. AH , JU, and PD constructed the energy diagrams. AH and JU drafted the original manuscript. JU and ST supervised the conduct of this

study. All authors reviewed the manuscript draft and revised it critically on intellectual content. All authors approved the final version of the manuscript to be published. ‡These authors contributed equally.

Funding Sources

JSPS KAKENHI (18KK0405, 20H02438)

ACKNOWLEDGMENT

This research was financially supported by JSPS KAKENHI (grant number is 18KK0405, 20H02438).

REFERENCES

(1) Xu, J.; Tanabe, S. Persistent luminescence instead of phosphorescence: History, mechanism, and perspective. *J. Lumin.* **2019**, *205*, 581-620.

(2) Ueda, J. How to Design and Analyze Persistent Phosphors? *Bulletin of the Chemical Society of Japan* **2021**, *94* (12), 2807-2821.

(3) Matsuzawa, T.; Aoki, Y.; Takeuchi, N.; Murayama, Y. A new long phosphorescent phosphor with high brightness, $SrAl_2O_4:Eu^{2+},Dy^{3+}$. *J. Electrochem. Soc.* **1996**, *143* (8), 2670-2673.

(4) Dorenbos, P. Mechanism of persistent luminescence in Eu^{2+} and Dy^{3+} codoped aluminate and silicate compounds. *J. Electrochem. Soc.* **2005**, *152* (7), 107-110.

(5) Joos, J. J.; Korthout, K.; Amidani, L.; Glatzel, P.; Poelman, D.; Smet, P. F. Identification of Dy^{3+}/Dy^{2+} as Electron Trap in Persistent Phosphors. *Phys. Rev. Lett.* **2020**, *125* (3), 033001.

(6) Murazaki, Y.; Arai, K.; Ichinomiya, K. New Red Long Persistence Phosphor. *J. Illum. Engng. Inst. Jpn* **1999**, *83* (7), 445-446.

(7) Luo, H.; Bos, A. J. J.; Dorenbos, P. Charge Carrier Trapping Processes in RE_2O_2S (RE = La, Gd, Y, and Lu). *J. Phys. Chem. C* **2017**, *121* (16), 8760-8769.

(8) Lin, F.; Li, X.; Chen, C.; Pan, X.; Peng, D.; Luo, H.; Jin, L.; Zhuang, Y.; Xie, R.-J. Modeling Polyhedron Distortion for Mechanoluminescence in Mixed-Anion Compounds $RE_2O_2S:Ln^{3+}$. *Chem. Mater.* **2022**, *34* (11), 5311-5319.

(9) Randall, J. T.; Wilkins, M. H. F. Phosphorescence and Electron Traps. II. The Interpretation of Long-Period Phosphorescence. *Proc. Roy. Soc. A Math. Phys. Sci.* **1945**, *184* (999), 390-407.

(10) Randall, J. T.; Wilkins, M. H. F. Phosphorescence and Electron Traps. I. The Study of Trap Distributions. *Proc. Roy. Soc. A Math. Phys. Sci.* **1945**, *184* (999), 365-389.

(11) Bos, A. J. J. Theory of Thermoluminescence. *Rad. Meas.* **2007**, *41* (0), S45-S56.

(12) Yokono, S.; Imanaga, S.; Hoshina, T. Raman Spectra for Eu Doped Ln_2O_2S Phosphors. *J. Phys. Soc. Jpn.* **1979**, *46* (6), 1882-1888.

(13) Dorenbos, P. The hole picture as alternative for the common electron picture to describe hole trapping and luminescence quenching. *J. Lumin.* **2018**, *197*, 62-65.

(14) Dorenbos, P.; Bos, A. J. J.; Poolton, N. R. J. Carrier recombination processes and divalent lanthanide spectroscopy in $YPO_4:Ce^{3+};L^{3+}$ (L=Sm,Dy,Tm). *Phys. Rev. B* **2010**, *82* (19).

(15) Korthout, K.; Van den Eeckhout, K.; Botterman, J.; Nikitenko, S.; Poelman, D.; Smet, P. F. Luminescence and x-ray absorption measurements of persistent $SrAl_2O_4$:Eu,Dy powders: Evidence for valence state changes. *Phys. Rev. B* **2011**, *84* (8), 085140.

(16) Ueda, J.; Katayama, M.; Asami, K.; Xu, J.; Inada, Y.; Tanabe, S. Evidence of valence state change of Ce^{3+} and Cr^{3+} during UV charging process in $Y_3Al_2Ga_3O_{12}$ persistent phosphors. *Optical Materials Express* **2017**, *7* (7), 2471-2476.

(17) Ueda, J.; Xu, J.; Takemura, S.; Nakanishi, T.; Miyano, S.; Segawa, H.; Tanabe, S. How Many Electron Traps are formed in Persistent Phosphors? *ECS J. Solid. State Sci. Technol.* **2021**, *10* (11), 116003.

(18) Dorenbos, P. The nephelauxetic effect on the electron binding energy in the $4f^q$ ground state of lanthanides in compounds. *J. Lumin.* **2019**, *214*, 116536.

(19) Dorenbos, P. [INVITED] Improved parameters for the lanthanide $4f^q$ and $4f^{q-1}5d$ curves in HRBE and VRBE schemes that takes the nephelauxetic effect into account. *J. Lumin.* **2020**, *222*, 117164.

(20) Malta, O. L.; Antic-Fidancev, E.; Lemaitre-Blaise, M.; Milicic-Tang, A.; Taibi, M. The crystal field strength parameter and the maximum splitting of the $^7F_1$ manifold of the Eu^{3+} ion in oxides. *J. Alloys Compd.* **1995**, *228* (1), 41-44.

(21) Moune, O. K.; Porcher, P.; Caro, P. A new analysis of the fluorescence spectrum of Eu^{3+} in A-type La_2O_3. *J. Solid State Chem.* **1983**, *50* (1), 41-50.

(22) Antic-Fidancev, E.; Hölsä, J.; Lastusaari, M.; Lupei, A. Dopant-host relationships in rare-earth oxides and garnets doped with trivalent rare-earth ions. *Phys. Rev. B* **2001**, *64* (19), 195108.

(23) Tanner, P. A.; Yeung, Y. Y.; Ning, L. What Factors Affect the $^5D_0$ Energy of Eu^{3+}? An Investigation of Nephelauxetic Effects. *J. Phys. Chem. A* **2013**, *117* (13), 2771-2781.

(24) Frey, S. T.; Horrocks, W. D. On correlating the frequency of the $^7F_0 \rightarrow {}^5D_0$ transition in Eu^{3+} complexes with the sum of 'nephelauxetic parameters' for all of the coordinating atoms. *Inorg. Chim. Acta* **1995**, *229* (1), 383-390.

(25) Albin, M.; Horrocks, W. D. Europium(III) luminescence excitation spectroscopy. Quantitive correlation between the total charge on the ligands and the $^7F_0 \rightarrow {}^5D_0$ transition frequency in europium(III) complexes. *Inorg. Chem.* **1985**, *24* (6), 895-900.

(26) Caro, P.; Beaury, O.; Antic, E. L'effet néphélauxétique pour les configurations $4f^N$ en phase solide. *J. Phys. France* **1976**, *37* (6), 671-676.

(27) Momma, K.; Izumi, F. VESTA 3 for three-dimensional visualization of crystal, volumetric and morphology data. *J. Appl. Crystallogr.* **2011**, *44* (6), 1272-1276.

(28) Yokono, S.; Abe, T.; Hoshina, T. Red luminescence of Ce^{3+} due to the large stokes shifts in Y_2O_2S and Lu_2O_2S. *J. Lumin.* **1981**, *24-25*, 309-312.

(29) Dorenbos, P. Modeling the chemical shift of lanthanide 4f electron binding energies. *Phys. Rev. B* **2012**, *85* (16), 165107.

TOC

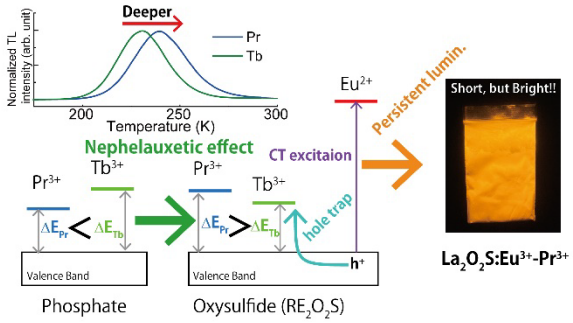
Deeper
Normalized TL intensity (arb. unit)
Pr
Tb
200
250
300
Temperature (K)
Nephelauxetic effect
CT excitaion
Eu2+
Persistent lumin.
Short, but Bright!!
Pr3+
Tb3+
Pr3+
Tb3+
ΔEPr < ΔETb
ΔEPr > ΔETb
hole trap
h+
Valence Band
Valence Band
La2O2S:Eu3+-Pr3+
Phosphate
Oxysulfide (RE2O2S)